Apoptosis (2019) 24:95–107
https://doi.org/10.1007/s10495-018-1496-1

# Klotho modulates ER-mediated signaling crosstalk between prosurvival autophagy and apoptotic cell death during LPS challenge

**Jennifer Mytych[1,2] · Przemyslaw Solek[1,2] · Marek Koziorowski[1,2]**

Published online: 24 October 2018


**Abstract**
Bacterial endotoxins have been shown to induce prosurvival autophagy or apoptosis in fibroblasts and thus impair the wound healing process. Endoplasmic reticulum has been proposed as a molecular switch between these processes and klotho protein possessing pleiotropic characteristics seems to be involved in both processes, however the exact molecular mechanism is unknown. In this study, we have evaluated the effect of *klotho* silencing on human fibroblasts exposed to a non-toxic dose of lipopolysaccharide in terms of in vitro wound healing ability. We show for the first time, that *klotho* silencing in fibroblasts intensified lipopolysaccharide-induced oxidative stress and inflammatory response, what resulted in genomic instability, p-eIF2a-mediated ER stress, retardation of prosurvival autophagy, induction of apoptotic cell death and finally in impaired wound closure. Therefore, our data suggest that klotho serves as a part of cellular defense mechanism engaged in providing protection against bacterial infections during wound healing by modulating ER-signaling crosstalk between autophagy and apoptosis.

**Keywords** Klotho · Fibroblasts · ER stress · Autophagy · LPS

## Introduction

Wound healing is a complex and dynamic physiological process for restoration of tissue integrity, traditionally explained in terms of three classic phases: inflammation, proliferation and maturation [1]. It is dependent on a number of inter-related factors and is particularly susceptible to infections [2] since the destruction of the skin barrier accelerates microbial invasion. The wound healing process may be significantly impacted by bacterial endotoxins, proteases, phospholipases and lipopolysaccharide (LPS), which may lead to prolonged inflammatory phase and development of skin or systemic infections as well as septic shock in the absence of effective decontamination [3]. LPS has been implicated in the pathogenesis of a number of skin diseases. Depending on the bacterial species and endotoxin level, LPS has been shown to differentially affect complete healing process as well as the functionality of main wound-repairing cells, i.e. fibroblasts and epithelial cells [4, 5]. It has been reported, that low, non-toxic levels of LPS accelerate proliferation and wound repair via Toll-like receptor 4 signaling cascade in epithelial cells [5] and induction of prosurvival autophagy pathways in fibroblasts [6, 7]. Normally, prosurvival autophagy allows degradation of damaged organelles or elimination of invading pathogens and thus is essential to maintain cellular homeostasis as well as limits inflammatory phase during the wound healing process [8]. On the other hand, toxic doses of LPS impact epithelial motility by altering the actin cytoskeleton and inducing overactivation of matrix metalloproteinase 2 [9], while in fibroblasts LPS induces apoptotic death through AKT/GSK3β pathway [10] and thus inhibits wound repair. However, the LPS-induced

**Electronic supplementary material** The online version of this article (https://doi.org/10.1007/s10495-018-1496-1) contains supplementary material, which is available to authorized users.

✉ Jennifer Mytych
jennifermytych@gmail.com

[1] Department of Animal Physiology and Reproduction, Faculty of Biotechnology, University of Rzeszow, Werynia 502, 36-100 Kolbuszowa, Poland

[2] Centre of Applied Biotechnology and Basic Sciences, University of Rzeszow, Werynia 502, 36-100 Kolbuszowa, Poland

crosstalk between autophagy and apoptosis appears to be extremely complex and recently endoplasmic reticulum (ER) has been proposed as a switch between cell survival and death. This is due to its high susceptibility to oxidative stress and an important role in the regulation of both mechanisms [11]. Nevertheless, the molecular mechanism is still unclear and further research is needed.

Impaired wound healing [12], autophagy [13] and ER stress [14] have been recently linked with anti-aging and anti-inflammatory protein klotho [15, 16]. In vivo studies have shown slower rate of wound closure in klotho mice (kl/kl), which has been linked partially with acute inflammation in wound lesions and depends on humoral factors [12, 17]. *Klotho* deficiency has also been correlated with an upregulated index of autophagy, increased collagen, decreased elastin content and arterial stiffening [13]. Further, elevated klotho levels have been shown to reduce expression of chemically induced ER stress markers, whilst loss of klotho has been casually linked to ER stress-induced apoptosis [14]. Also, klotho in vivo administration have ameliorated ER stress, inhibited the apoptotic process and attenuated fibrosis [18]. Taking into account mentioned klotho characteristics, we hypothesized that klotho could act as a molecular switch in modulating ER-signaling crosstalk between autophagy and apoptosis induced by LPS during the wound healing process. To date, one other study reported the role of klotho protein in autophagy and apoptosis control. Xie et al. have shown that klotho may inhibit IGF-1 signaling and subsequently induce apoptosis through downregulating PI3K-Akt-mTOR autophagy signaling [19]. However, this study was done in cancer cells and have not involved evaluation of ER stress mechanism.

Therefore, the aim of this study was to evaluate the effect of *klotho* silencing on normal human fibroblasts exposed to the non-toxic dose of LPS in terms of in vitro wound healing ability with the emphasis on oxidative stress- and proinflammatory cytokines-induced activation of autophagy and apoptotic pathways. This study will bring new, important insight into the LPS-challenged process of wound healing since impaired wound healing due to the bacterial infections is ongoing emerging and prevalent clinical problem.

## Materials and methods

### Materials

All reagents had analytical grade purity and unless otherwise stated, were purchased from Sigma. Antibodies catalogue numbers, TaqMan probes IDs and primer sequences are presented in the supplement.

### Cell culture, klotho silencing and LPS stimulation

Diploid human fibroblast cells, BJ cell line (ATCC), were cultured at 37 °C in a humidified atmosphere in the presence of 5% $CO_2$ in high-glucose DMEM with 1 mM sodium pyruvate, supplemented with 10% FBS and antibiotic mix solution (100 U/ml penicillin, 0.1 mg/ml streptomycin) and 29.2 mg/ml L-glutamine. For siRNA transfections, cells were seeded into 12-well plates at the density of $7.5 \times 10^3$ cells/cm$^2$ and after 24 h transfected with 10 pmol Ctrl-siRNA (Silencer Negative Control No. 1 siRNA; #AM4611, Thermo Scientific) or 10 pmol KLTH-siRNA (UniGeneID Hs.524953; siRNA ID 15391; #AM16708, Thermo Scientific-siRNA #1; UniGeneID Hs.524953; siRNA ID 15204; #AM16706, Thermo Scientific-siRNA #2) using 3 µl Lipofectamine RNAiMAX reagent (Thermo Scientific) and following standard manufacturer's protocol. Two days after transfection with Ctrl-siRNA or KLTH-siRNA, fibroblasts were trypsinized and seeded at the constant density of $3 \times 10^3$ cells/cm$^2$ and after 24 h treated with 1 µg/ml LPS from *E. coli* serotype 0055:B5 (Sigma, prepared in PBS). Cells were incubated with LPS for 48 h (unless otherwise stated) and then following experiments were performed.

### Wound repair assay

In each well of 12-well plate, $10^4$ cells were seeded, after 24 h scratch was done with 10 µl tip and the medium was replaced by fresh medium with 1 µg/ml LPS. Microphotographs were taken using Zeiss Axiovert 40CFL inverted microscope and a computer image analysis system Zeiss Axiovert 40CFL immediately after a scratch, after 24 and 48 h. Quantitative analysis was conducted with ImageJ software and results were presented as % of wound closure.

### MTT assay

After 48 h incubation with LPS, cell culture medium was removed and replaced with medium containing 500 µg/ml MTT for 4 h. Afterwards, the medium was discarded, crystals were dissolved in DMSO and the absorbance was read at 595 nm and 655 nm (measurement and reference wavelength, respectively) using PerkinElmer Victor X4 2030 microplate reader. The readings for the untreated Ctrl-siRNA cells were considered as 100%.

### Cell cycle distribution analysis and BrdU incorporation assay

For cell cycle evaluation, after 48 h incubation with LPS, cells were stained for 20 min at 37 °C with 1 µg/

ml Hoechst 33342 prepared in DMEM w/o FBS, washed twice with PBS and fluorescent images were taken with InCell Analyzer 2000. Analysis was conducted with DNA Cell Cycle plug-in from ImageJ software and results presented as % of cells in each of G0/G1, S and G2/M phases.

For BrdU incorporation assay, 10 µM BrdU was added to fibroblasts 6 h before fixation. Then, cells were washed with PBS, fixed in 4% paraformaldehyde for 15 min, permeabilized in PBS-T (PBS with 0.25% Triton-X) for 20 min, incubated for 60 min with 2 M HCl at 37 °C, blocked with 1% BSA and incubated overnight with anti-BrdU antibody (4 °C). Then, the secondary antibody was added and nuclei were visualized with Hoechst 33258 and digital images were taken with InCell Analyzer 2000. Positive cells were counted and presented as %, while the results obtained for the untreated control were considered as 100%.

## Real time PCR and reverse transcription PCR

Total RNA was extracted using Trizol reagent according to the protocol supplied by the manufacturer (Thermo Scientific). Then, 2 µg of RNA was reverse transcribed to cDNA with High-Capacity cDNA Reverse Transcription Kit and TaqMan gene expression assays were performed with 10 ng cDNA according to provided instructions (Applied Biosystems). *CREB* and *KLTH* genes expression levels were determined using the $2^{-\Delta\Delta CT}$ method after normalization with the mean of the two housekeeping genes (*18S* and *ACTB*).

The reverse transcription PCR was performed with 2xPCR TaqNova-RED master mix (DNA Gdansk), reverse and forward primers for *XBP-1* or *ACTB* (10 pmol) and 50 ng cDNA. The amplification of PCR was carried out for 35 cycles of denaturing at 95 °C for 45 s, annealing at 57 °C for 45 s and extension at 72 °C for 45 s, followed by final extension at 72 °C for 10 min. PCR products were electrophoretically detected on 3% agarose gel after staining with ethidium bromide.

## Intracellular zinc ($Zn^{2+}$) and calcium ($Ca^{2+}$) pools detection

Cells were trypsinized and suspended at the density of $2 \times 10^5$/ml in HBSS and 2 µM of the fluorescent probe was added for 15 min at 37 °C (Zinquil ethyl ester for $Zn^{2+}$ or Fura-PE3AM for $Ca^{2+}$ detection, Cayman Chemical). Fluorescence intensity was measured in PerkinElmer Victor X4 2030 microplate reader ($\lambda_{ex} = 368$ nm, $\lambda_{em} = 490$ nm-Zinquin ethyl ester; 335 nm/364 nm ratio-Fura-PE3AM). Results are presented as RFU ($Zn^{2+}$) and as ratio $F_{335}/F_{364}$ ($Ca^{2+}$).

## Oxidative stress and nitric oxide level measurement

Superoxide, nitric oxide and reduced glutathione levels were estimated using fluorogenic redox-sensitive probes: dihydroethidium, 4-amino-5-methylamino-2′,7′-difluorofluorescein diacetate and Thiol Tracker Violet (Thermo Scientific), respectively, as described in manufacturer's protocols. Digital images were captured with InCell Analyzer 2000, quantitative analysis was conducted with InCell Analyzer analysis module and results are presented as RFU.

## Enzyme-linked immunosorbent assay (ELISA)

Levels of secreted tumor necrosis factor α (TNFα) (#EH3TNFA; Lot 1711982A), interleukin 1β (IL-1β) (#EH2IL1B; Lot 1720202A), interleukin 6 (IL-6) (#EH2IL6; Lot 1697169A) and interleukin 10 (IL-10) (#EHIL10; Lot 1742850A) in supernatants were determined using ELISA kits (Thermo Scientific) according to provided instructions. The results were normalized to cell numbers. The readings for the untreated Ctrl-siRNA cells were considered as 100%.

## Western blot

Whole cell protein lysates were prepared and Western Blot was performed according to Mytych et al. [15, 20]. Briefly, 20 µg of proteins was separated by 10% SDS–PAGE and electroblotted to PVDF membranes, followed by blocking in 1% BSA, incubated with the specific primary and secondary HRP-conjugated antibodies. The protein bands of interest were detected using ECL substrate (Bio Rad) and Fusion Fx7 system (Viber Lourant). The relative protein expression levels were normalized to β-actin (GelQuantNET software).

## Immunofluorescence staining and micronuclei (MN) detection

Immunostaining protocols were used as described previously [15, 20, 21]. In contrast to intracellular immunostaining procedure, all buffers used in cell surface (extracellular) immunostaining method were Triton X-free. Digital images were captured with InCell Analyzer 2000. ImageJ software was used for quantitative analysis of klotho abundance (results are presented as RFU) and γH2AX foci formation (shown as γH2AX foci/nucleus). For micronuclei analysis, minimum of 500 cells were examined for each sample and results are presented as MN % of total cells.

## Autophagy detection: acridine orange staining and LC3 puncta immunostaining

As a marker of autophagy, the volume of the cellular acidic compartment was visualized by acridine orange (AO)

staining. The AO stain crosses into lysosomes and becomes protonated. The protonated dye stacks and stacked AO emits red fluorescence, while AO not in acidic compartment emits as green [22]. To visualize autophagosomes, cells were stained for 15 min at 37 °C with 1 µg/ml acridine orange prepared in DMEM and washed twice with PBS. AO assay is only a supplementary method due to its high affinity to other acidic compartments, therefore the second method of autophagy detection was employed i.e. LC3 puncta immunostaining. The intracellular LC3 puncta immunostaining was done as described above in immunofluorescence staining protocol. Digital images were taken with InCell Analyzer 2000 and analyzed with InCell Analyzer analysis module and presented as RFU and LC3 puncta / cell, respectively.

### Statistical analysis

Analyses were performed on GraphPad Prism. Unless otherwise stated, data from at least three independent experiments ($n = 3$) are presented as mean ± SD and analyzed with one-way ANOVA with Dunnett's multiple comparison post test. p values $< 0.05$ were considered significant (***/^^^$p < 0.001$; **/^^$p < 0.01$; */^$p < 0.05$, no indication—no statistical significance). (*) indicate a comparison between LPS-non-treated and treated Ctrl-siRNA or KLTH-siRNA cells, (^) indicate a comparison between LPS-non treated Ctrl-siRNA and KLTH-siRNA cells or LPS-treated Ctrl-siRNA and KLTH-siRNA cells.

## Results

### Klotho siRNA-mediated cell cycle arrest and apoptosis induction is involved in in vitro wound healing inhibition during LPS challenge

To verify the role of klotho protein in LPS-challenged wound healing process we firstly silenced *klotho* gene in BJ cells using siRNA strategy. For this reason, we used two different siRNAs, however with opposite results. Cells transfected with *klotho* siRNA #1 did not exhibit decreased expression of klotho in both, mRNA and protein, levels (Fig. 1). On the other hand, cells transfected with *klotho* siRNA #2 showed lower expression of *klotho*. As assessed by real time PCR, *klotho* expression decreased by 62% ($p < 0.001$) (Fig. 1a). Transmembrane klotho (130 kDa) protein levels following 48 h siRNA silencing dropped by 73.9% when compared to cells transfected with negative control siRNA (Ctrl-siRNA) ($p < 0.01$), as well as levels of secrete form of klotho protein (65 kDa) were reduced as assessed by Western Blot technique (Fig. 1b, c). Therefore, for further experiments, we decided to continue with siRNA #2, which gave high efficiency in *klotho* silencing.

After silencing the *klotho* gene in BJ cells (KLTH-siRNA), we decided to check whether this process will affect wound healing challenged for 48 h with non-toxic LPS dose (1 µg/ml). Indeed, during 2 days of analysis, the percentage wound closure in Ctrl-siRNA cells treated with LPS was 99.6% with no difference when compared to non-treated cells (96.9%). Whereas in KLTH-siRNA cells wound healing process was not only slightly slowed down (84.0%, $p > 0.05$, ns), but LPS challenge additionally intensified that deceleration to 56.6% ($p < 0.001$) (Fig. 2a, b). We next wanted to investigate whether the observed effects after LPS treatment were due to their impact on cell cycle and proliferation

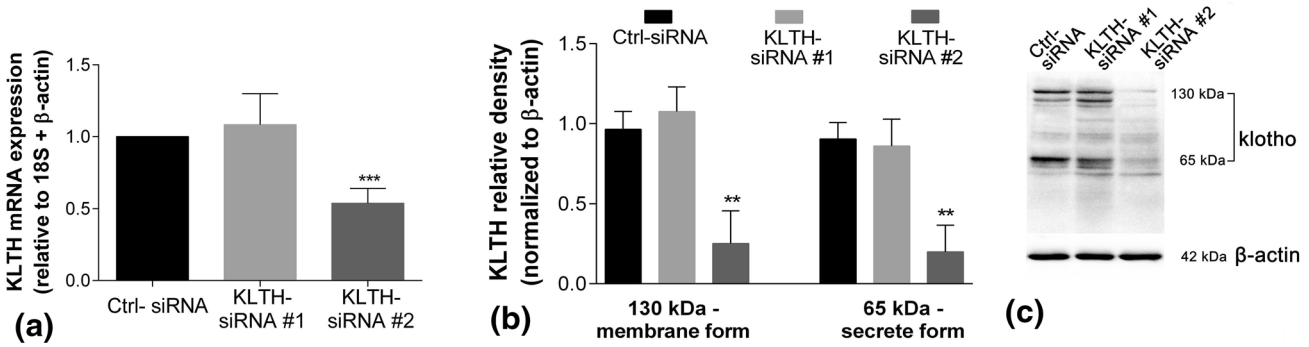


**Fig. 1** siRNA-mediated *klotho* silencing of normal human fibroblasts. Cells were transfected with 10 pmol Silencer Negative Control (Ctrl-siRNA) or 10 pmol klotho siRNA (KLTH-siRNA #1 and #2) for 48 h. **a** qPCR analysis of klotho mRNA expression; **b** Western Blot analysis of klotho membrane (130 kDa) and secrete (65 kDa) forms expression after transfection, **c** representative Western Blots are shown; Bars indicate SD, $n = 3$, ***$p < 0.001$, **$p < 0.01$ (one-way ANOVA and Dunett's a posteriori test)

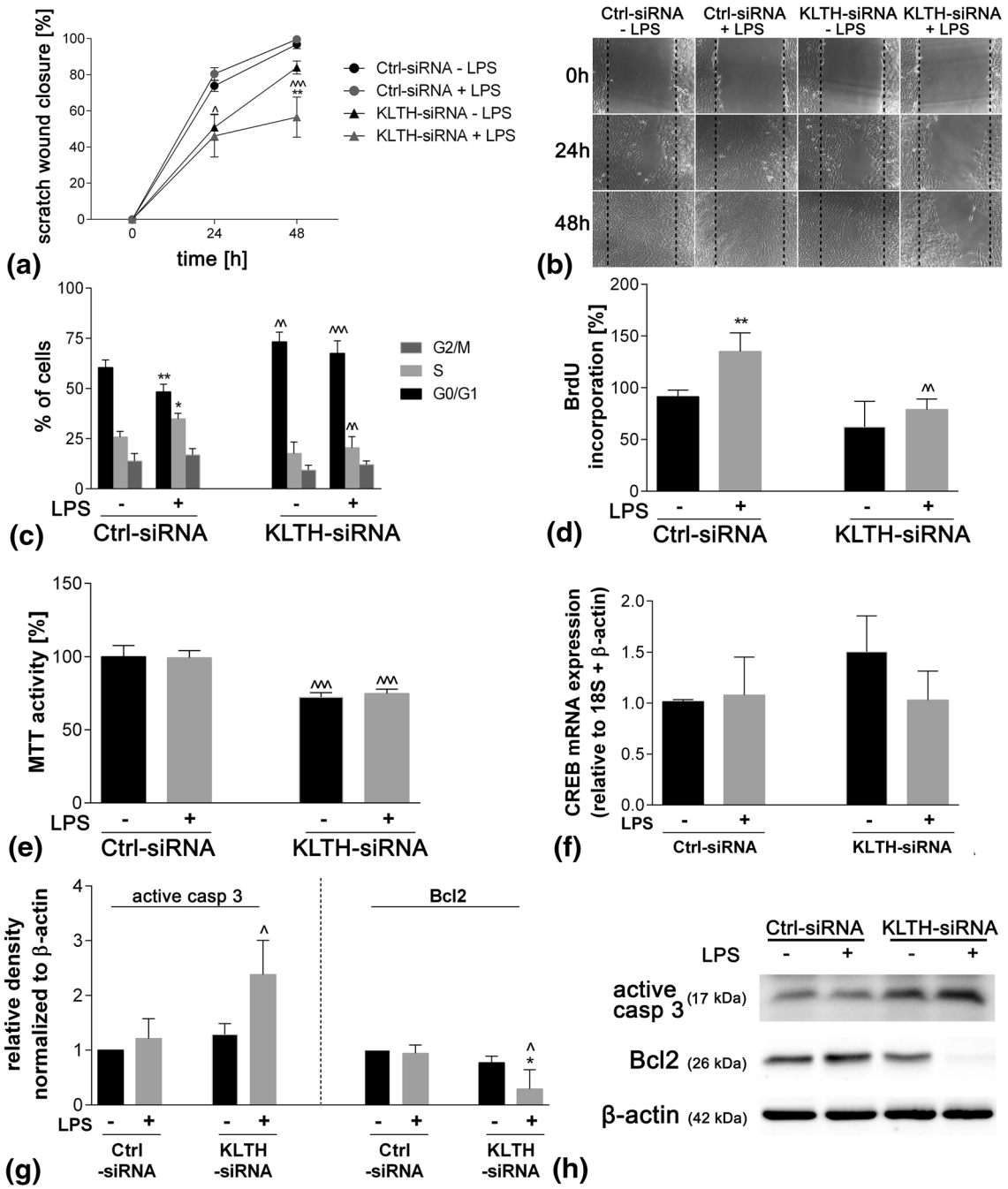


**Fig. 2** Klotho siRNA-mediated inhibition in wound healing process during LPS challenge is associated with decreased proliferation capacity, cell cycle arrest and apoptosis induction. **a** Scratch assay. 48 h after transfection, cells were seeded, after next 24 h scratch was done and LPS (1 µg/ml) was added (0 h). Wound closure was controlled at 0 h, 24 and 48 h; **b** representative images are presented, magnification of the objective lens 20×; 48 h after transfection, cells were seeded, after next 24 h treated with LPS and **c** cell cycle progression was evaluated; **d** BrdU incorporation was controlled; **e** MTT activity was measured; **f** CREB expression was evaluated; **g** apoptosis-associated active caspase 3 and Bcl-2 expression was controlled, **h** representative Western Blots are shown. Bars indicate SD, n = 3, ***/^^^p < 0.001, **/^^p < 0.01, */^p < 0.05, no indication—no statistical significance (one-way ANOVA and Dunett's a posteriori test). (*) indicate comparison between LPS-non-treated and treated Ctrl-siRNA or KLTH-siRNA cells, (^) indicate comparison between LPS-non treated Ctrl-siRNA and KLTH-siRNA cells or LPS-treated Ctrl-siRNA and KLTH-siRNA cells

rate. Firstly, *klotho* silencing led to the cell cycle arrest in G0/G1 phase. Then, the % of LPS non-challenged KLTH-siRNA cells in G0/G1 phase was increased by 12.7% when compared to Ctrl-siRNA cells ($p < 0.01$), while in LPS challenged cells the observed increase was 19.2% ($p < 0.001$). In terms of S phase, the % of Ctrl-siRNA cells increased by 9.0% due to the LPS treatment ($p < 0.05$), however in KLTH-siRNA cells we did not observe the same tendency (Fig. 2c). This data was supported by results obtained in BrdU incorporation test (Fig. 2d). Further, we noted decreased MTT activity in KLTH-siRNA cells independently on LPS treatment (in Ctrl-siRNA cells ~ 100% and in KLTH-siRNA cells ~ 73%, $p < 0.001$) (Fig. 2e), which could be due to the reduced cell or mitochondrial number as well as metabolic activity. Since, no statistically significant differences in *CREB*, the master regulator of mitochondrial biogenesis, expression were observed (Fig. 2f), reduction in MTT activity should be considered as a consequence of decreased cell number. Apart from proliferation rate inhibition and G0/G1 cell cycle arrest, apoptotic cell death induction could be also involved in the observed decrease in cell number. Therefore, we evaluated the levels of Bcl2 and active caspase 3—two proteins regulating apoptotic cascade. In Ctrl-siRNA cells treated with LPS, we did not observe any changes in their pattern. On the other hand, in KLTH-siRNA cells challenged with LPS, we noted the increased level of active caspase 3 ($p < 0.05$) with a concomitant drop in Bcl2 amount suggesting activation of apoptotic pathway ($p < 0.05$) (Fig. 2g, h).

## Klotho siRNA increases LPS-mediated oxidative stress and imbalance in intracellular zinc and calcium homeostasis in fibroblasts

To explore the molecular mechanism behind the reduction in wound healing ability of KLTH-siRNA fibroblasts challenged with LPS we evaluated oxidative and nitrosative stress parameters. We noted a 1.4-fold increase in superoxide production in Ctrl-siRNA cells after LPS treatment ($p < 0.01$), while *klotho* silencing intensified observed increase to 1.8-fold (Fig. 3a, b). Similarly, LPS challenge led to a 1.5-fold upregulation in nitric oxide generation in Ctrl-siRNA cells ($p < 0.001$), however in KLTH-siRNA cells no changes in nitric oxide pools were observed (Fig. 3c, d). Oxidative and nitrosative stress resulted in the employment of glutathione antioxidant system as observed by downregulation of thiol pools. The level of thiols reflecting reduced glutathione content was decreased approximately by 20% in Ctrl-siRNA ($p < 0.05$) and 32% in KLTH-siRNA cells ($p < 0.001$) after LPS treatment (Fig. 3e, f). Also, as an adaptive response, we noted activation of NF-κB transcription factor and IGF-IR pathways due to LPS challenge in Ctrl-siRNA cells and the effect was even more pronounced in KLTH-siRNA cells. Simultaneously, in Ctrl-siRNA fibroblasts LPS did not promote any changes in heme oxygenase 1 (HMOX-1) or heme oxygenase 2 (HMOX-2) protein pools, however in KLTH-siRNA cells upregulation of HMOX-1 was observed ($p < 0.05$). Further, although antioxidant systems were activated, LPS treatment resulted in increased protein O-GlcNAcylation and in KLTH-siRNA cells O-GlcNAc modification of proteins with high molecular weight (> 90 kDa) was enhanced by approximately 1.5-fold ($p < 0.01$) when compared to Ctrl-siRNA fibroblasts (Fig. 3g–i). Inseparably linked to oxidative and nitrosative stress is imbalance in intracellular zinc and calcium amounts. LPS challenge led to a 1.8-fold increase in $Ca^{2+}$ pool in Ctrl-siRNA cells ($p < 0.01$), while KLTH-siRNA cells were unaffected (Fig. 3j). Slight decrease in $Zn^{2+}$ amount after treatment with LPS in both, Ctrl-siRNA and KLTH-siRNA fibroblasts, was noted (Fig. 3k), probably due to the upregulated zinc transporter ZnT1 presence (Fig. 3g, i).

## Klotho siRNA increases inflammation in fibroblasts challenged with LPS

Changes in intracellular available zinc/calcium and oxidative stress are intimately related with inflammatory response what could further explain the molecular mechanism behind the reduction in wound healing ability of KLTH-siRNA fibroblasts challenged with LPS. Therefore, we evaluated levels of both, pro- and anti-inflammatory cytokines. LPS treatment resulted in 157% increase in TNFα secretion in Ctrl-siRNA cells ($p < 0.05$), while in KLTH-siRNA fibroblasts 296% upregulation was observed ($p < 0.01$). However, the basal level of TNFα secretion was also increased by 108% due to *klotho* silencing and was LPS-independent ($p < 0.05$) (Fig. 4a). IL-6 profile was affected in LPS-treated KLTH-siRNA cells ($p < 0.05$) (Fig. 4b), whereas IL-1β secretion was upregulated by 88% ($p < 0.05$) and 135% ($p < 0.05$) in Ctrl-siRNA and KLTH-siRNA cells, respectively (Fig. 4c). The levels of secreted anti-inflammatory IL-10 were also changed. LPS challenge led to enhancement of IL-10 secretion by 72% in Ctrl-siRNA cells ($p > 0.05$, ns). However, when compared LPS treated Ctrl-siRNA and KLTH-siRNA cells, statistically significant downregulation in IL-10 secretion was observed in cells with silenced *klotho* ($p < 0.05$) (Fig. 4d).

## Klotho silencing enhances ER stress and induces genomic instability in fibroblasts challenged with LPS

Excessive protein O-GlcNAcylation could also lead to unfolded protein response (UPR) in response to accumulation of unfolded or misfolded proteins in ER. This theory is supported by simultaneously observed LPS-induced oxidative stress and increased inflammatory response in

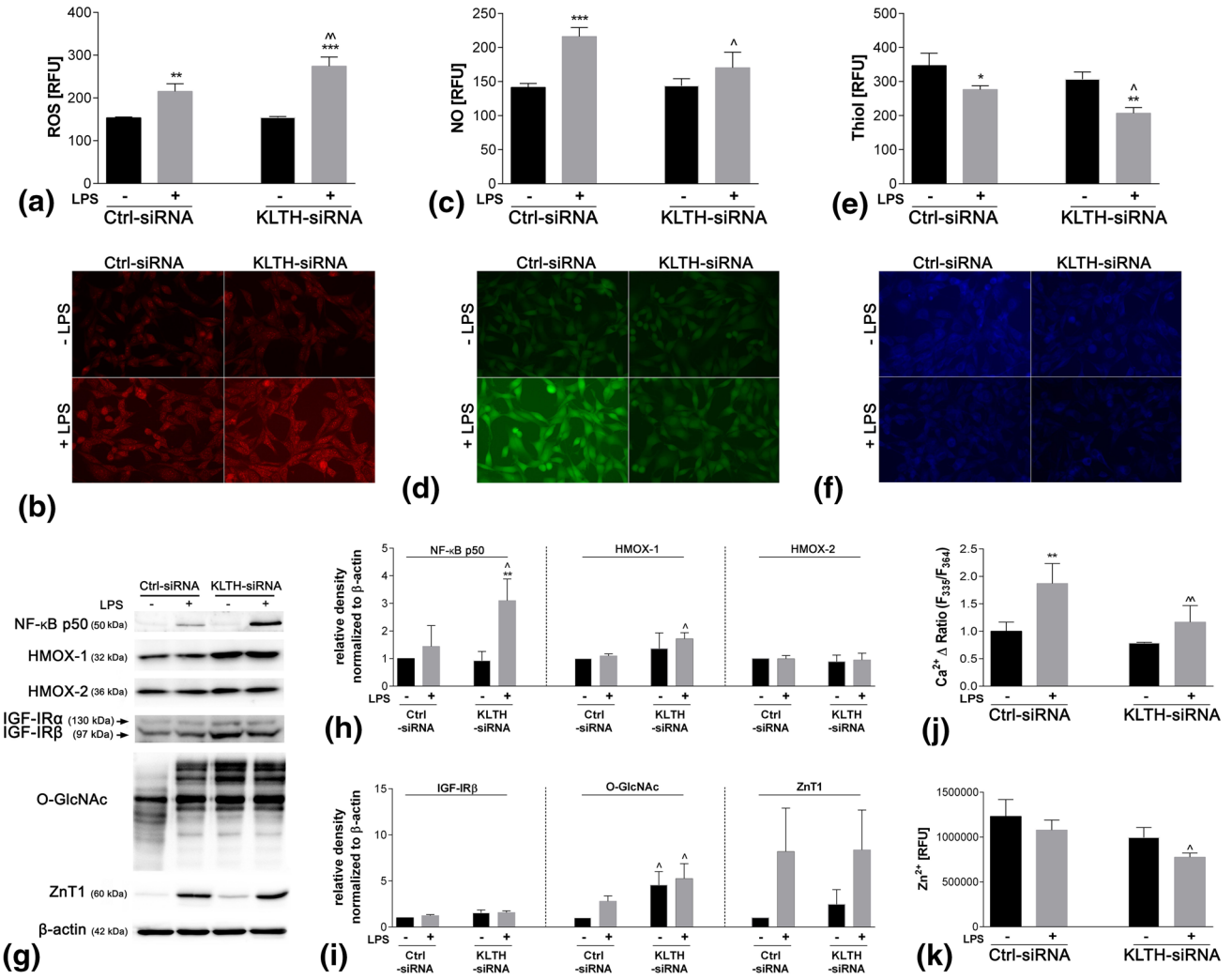


**Fig. 3** Klotho siRNA increases LPS-mediated oxidative stress and imbalance in intracellular zinc and calcium homeostasis in fibroblasts. 48 h after transfection, cells were seeded, after next 24 h treated with LPS and after 48 h **a** ROS levels; **b** representative images; **c** NO levels, **d** representative images; **e** Thiol levels, **f** representative images were controlled. Magnification of the objective lens 20×. Red fluorescence—dihydroethidium (ROS), green—4-amino-5-methylamino-2′,7′-difluoro-fluorescein diacetate (NO), blue fluorescence—Thiol Tracker (Thiol); **g** activation of anti-oxidant pathways and extent of O-GlcNAcylation were controlled, representative Western Blots are shown; **h** densitometry analysis of NF-κB p50, HMOX-1, HMOX-2 and **i** IGF-IR, O-GlcNAc, ZnT1. **j** $Ca^{2+}$ and **k** $Zn^{2+}$ intracellular pools were measured. Bars indicate SD, n = 3, ***/^^^p < 0.001, **/^^p < 0.01, */^p < 0.05, no indication—no statistical significance (one-way ANOVA and Dunett's a posteriori test). (*) indicate comparison between LPS-non-treated and treated Ctrl-siRNA or KLTH-siRNA cells, (^) indicate comparison between LPS-non treated Ctrl-siRNA and KLTH-siRNA cells or LPS-treated Ctrl-siRNA and KLTH-siRNA cells. (Color figure online)

KLTH-siRNA cells. Therefore, we investigated two parallel signaling branches comprised by UPR. In both, Ctrl-siRNA and KLTH-siRNA cells LPS challenge did not lead to splicing of X-box binding protein-1 (XBP-1) mRNA (Fig. 5a, b). However, we confirmed a 1.06-fold increase in eukaryotic translation initiation factor 2A phosphorylation (p-eIF2a) in Ctrl-siRNA cells treated with LPS, whilst in KLTH-siRNA cells a 2.76-fold upregulation was observed ($p < 0.01$). Since we observed apoptosis induction in KLTH-siRNA cells challenged with LPS and calnexin is known to be involved in apoptosis induced by ER stress, we evaluated the levels of its expression. Indeed, we confirmed 1.57- ($p > 0.05$, ns) and 3.45-fold ($p < 0.05$) increases in calnexin expression in Ctrl-siRNA and KLTH-siRNA cells, respectively after treatment with LPS (Fig. 5c, d). ER stress was recently linked with genomic instability and here we observed increased micronuclei formation in LPS-treated KLTH-siRNA cells when compared to Ctrl-siRNA cells ($p < 0.01$) (Fig. 5e, f). Simultaneously, a 2.39-fold increase in DNA double strand brakes, as assessed by γH2AX foci formation analysis, was observed in KLTH-siRNA cells after LPS treatment when

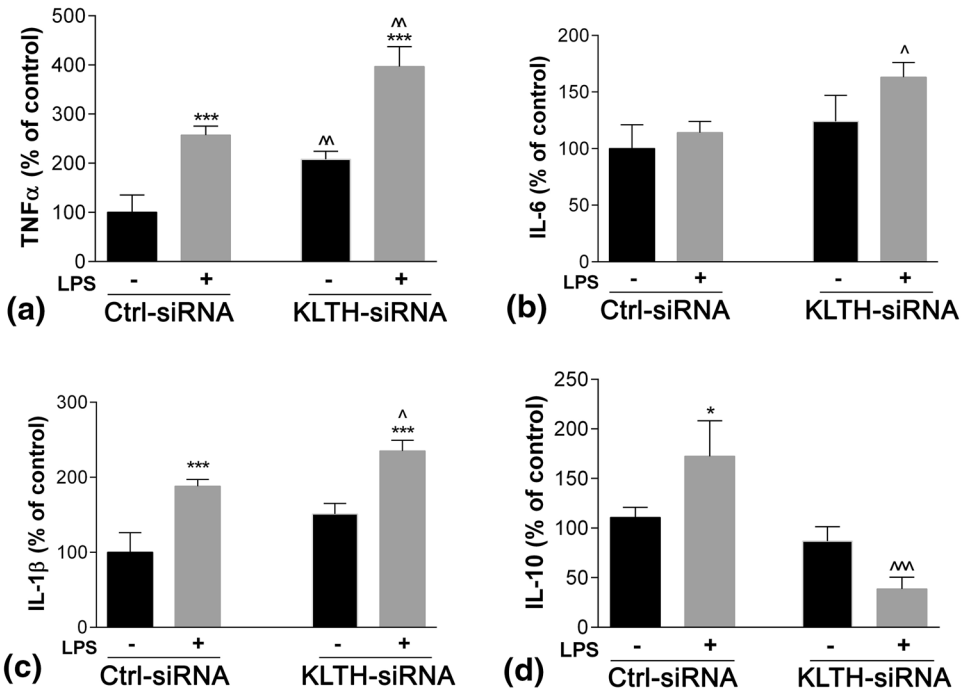


**Fig. 4** Klotho siRNA increases inflammation in fibroblasts challenged with LPS. 48 h after transfection, cells were seeded, after next 24 h treated with LPS and **a** TNFα **b** IL-6 **c** IL-1β and **d** IL-10 secretion was measured. Bars indicate SD, n = 2, ***/^^^p < 0.001, **/^^p < 0.01, */^p < 0.05, no indication—no statistical significance (one-way ANOVA and Dunett's a posteriori test). (*) indicate comparison between LPS-non-treated and treated Ctrl-siRNA or KLTH-siRNA cells, (^) indicate comparison between LPS-non treated Ctrl-siRNA and KLTH-siRNA cells or LPS-treated Ctrl-siRNA and KLTH-siRNA cells

compared to Ctrl-siRNA fibroblasts ($p < 0.001$). Interestingly, detailed analysis revealed that γH2AX foci showed differential labeling-pattern. Some of them were localized only in micronucleus and not in the nucleus, some in both, while some others only in the nucleus (Fig. 5g, h).

### Klotho siRNA leads to autophagy repression and thus inhibits wound healing ability during LPS challenge

Mild ER stress mediates autophagy initiation required for cytoprotection, thus in the next step of our study, we evaluated autophagy pathway activation as a response to LPS challenge. We detected a 65.2% increase in acridine orange staining intensity reflecting acidic compartments in Ctrl-siRNA cells after treatment with LPS ($p < 0.05$), while in KLTH-siRNA fibroblasts observed upregulation was 25.7% ($p > 0.05$, ns) (Fig. 6a, b). To confirm autophagy activation, we used more specific method i.e. LC3 puncta immunostaining and noted a 3.3-fold LPS-induced increase in LC3 puncta formation per cell in Ctrl-siRNA cells ($p < 0.01$), whilst in KLTH-siRNA the same tendency was not observed (Fig. 6c, d). Immunoblotting with an antibody against LC3A/B additionally confirmed these observations. Furthermore, we observed 63% downregulation in ATG16L synthesis ($p < 0.001$), the protein crucial for autophagosome formation, in KLTH-siRNA cells treated with LPS, while ATG16L pools in Ctrl-siRNA fibroblasts were unaffected even after LPS challenge (Fig. 6e, f).

## Discussion

Recently published in vivo studies showed a slower rate of wound closure in klotho mice (kl/kl), which was partially linked with acute inflammation in wound lesions and depended on humoral factors [12, 17]. However, the molecular mechanisms underlying the complex and multistage wound healing process associated with *klotho* deficiency were not completely understood. One of the most important and intriguing unanswered question was the effect of interactions between wounds and microbia / endotoxins. In this study, we confirmed that overall in vitro wound healing process outcome was not affected in normal human fibroblasts challenged with non-toxic dose of LPS, what is in agreement with others [4, 23], whereas *klotho* silencing resulted in significantly reduced wound closure. Additionally, we report the precise mechanism underlying these interactions.

In *klotho* silenced fibroblasts challenged with LPS production of ROS and NF-κB activation were significantly intensified. The effect was additionally augmented by depletion of reduced glutathione. To date, klotho role in oxidative stress was well described [24, 25]. Moreover, some evidence is emerging that klotho modulates inducible nitric oxide synthase (iNOS) activity and its deficiency causes the reduction in NO and cGMP [26]. Similarly, in our study, we observed significantly decreased NO production due to the LPS treatment in fibroblasts with *klotho* silenced. This observation is particularly significant in terms of wound healing process since NO release through iNOS regulates collagen formation, cell

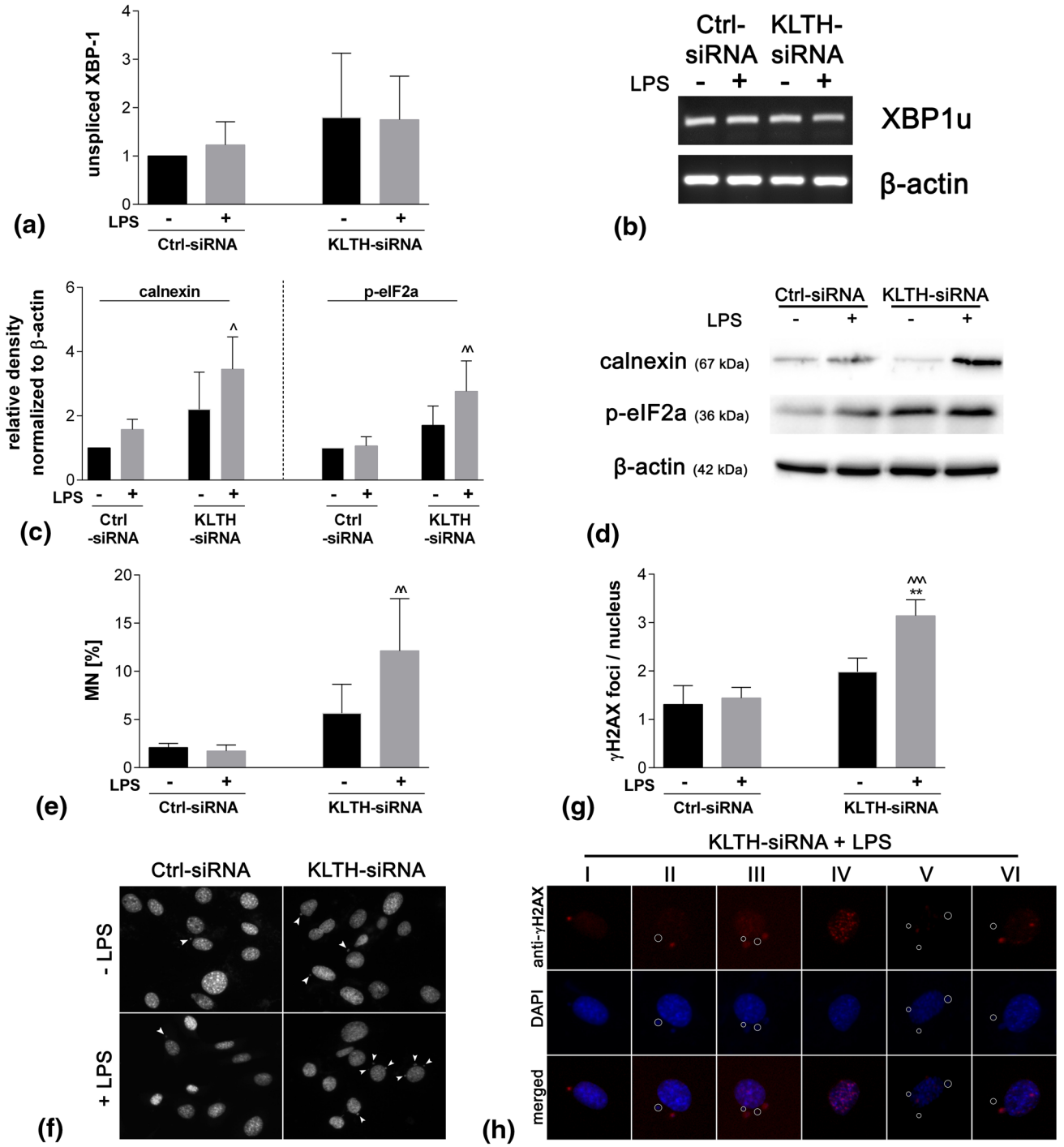


**Fig. 5** Klotho silencing enhances endoplasmic reticulum stress in fibroblasts challenged with LPS. 48 h after transfection, cells were seeded, after next 24 h treated with LPS and **a** XBP-1 splicing was evaluated, **b** representative image of the PCR products after agarose gel electrophoresis; **c** expression of calnexin and p-eIF2a involved in ER-stress was controlled, **d** representative Western Blots are shown; **e** micronuclei formation was monitored, **f** representative photos after DAPI staining are presented; **g** γH2AX foci formation was controlled, **h** representative images are presented, foci localized in I—micronucleus, II and III—one of micronuclei, IV—nucleus, V—nucleus and not micronucleus, VI—both, nucleus and micronucleus, magnification of the objective lens 20×. Bars indicate SD, n = 3, ***/^^^p < 0.001, **/^^p < 0.01, */^p < 0.05, no indication—no statistical significance (one-way ANOVA and Dunett's a posteriori test). (*) indicate comparison between LPS-non-treated and treated Ctrl-siRNA or KLTH-siRNA cells, (^) indicate comparison between LPS-non treated Ctrl-siRNA and KLTH-siRNA cells or LPS-treated Ctrl-siRNA and KLTH-siRNA cells

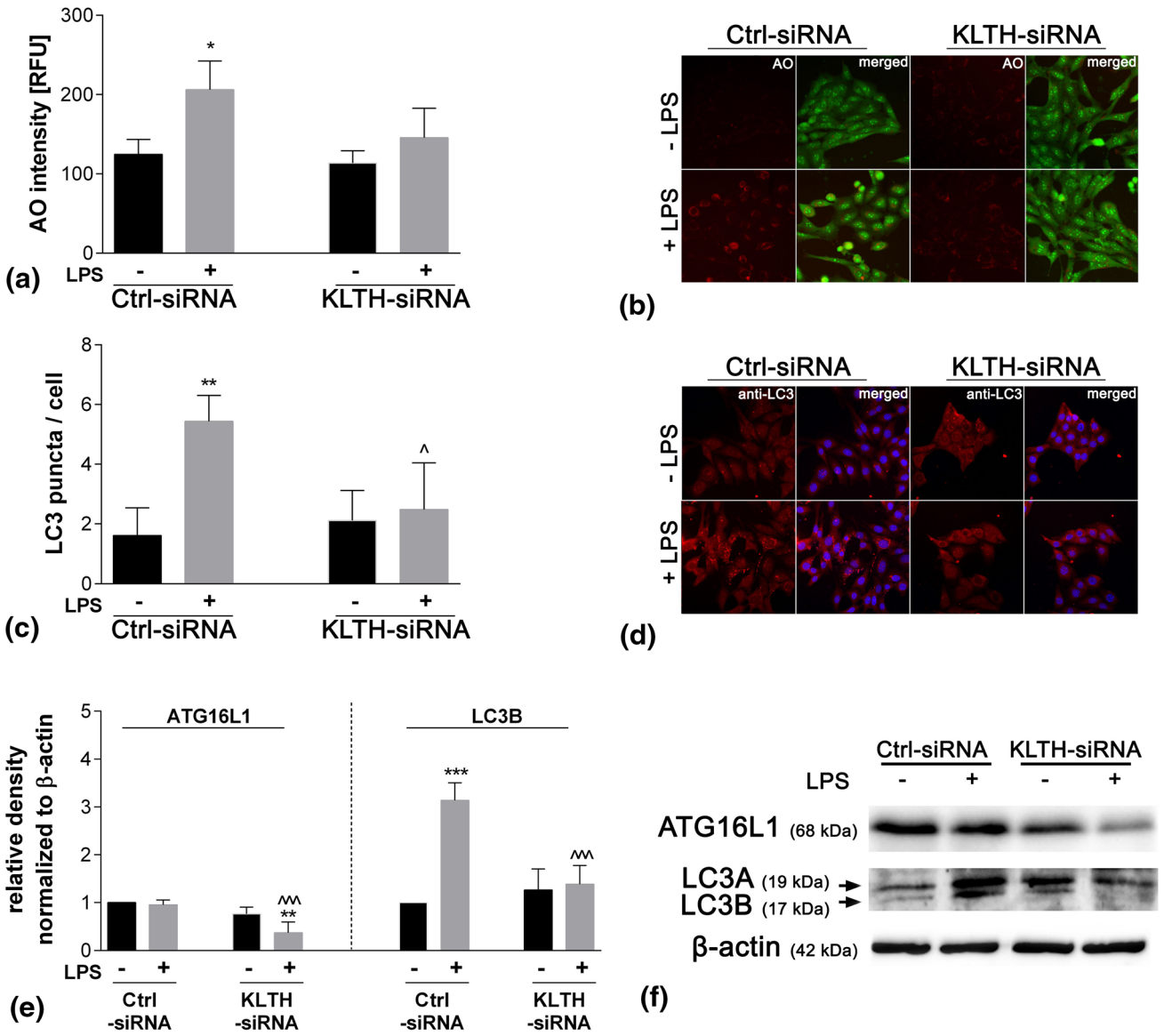


**Fig. 6** Klotho siRNA leads to autophagy repression and thus inhibits wound healing ability during LPS challenge. 48 h after transfection, cells were seeded, after next 24 h treated with LPS and **a** orange acridine staining was performed, **b** representative photos are presented, magnification of the objective lens 20×. Red fluorescence—acidic compartments, green—cytoplasm; **c** LC3 puncta immunostaining was done, **d** representative photos are presented, magnification of the objective lens 20×. Red fluorescence—Texas Red (LC3); blue—Hoechst 33342 (nuclei); **e** expression of LC3A/B and ATG16L associated with autophagy process, **f** representative Western Blots are shown. Bars indicate SD, n = 3, ***/^^^p < 0.001, **/^^p < 0.01, */^p < 0.05, no indication—no statistical significance (one-way ANOVA and Dunett's a posteriori test). (*) indicate comparison between LPS-non-treated and treated Ctrl-siRNA or KLTH-siRNA cells, (^) indicate comparison between LPS-non treated Ctrl-siRNA and KLTH-siRNA cells or LPS-treated Ctrl-siRNA and KLTH-siRNA cells. (Color figure online)

proliferation and wound contraction [27], thus reduced NO level may also indirectly explain reduced proliferation in *klotho* silenced fibroblasts challenged with LPS. Inhibition of LPS-mediated expression of NO could be also associated with observed enhanced O-GlcNAcylation. Additionally, noted in this study decrease in calcium influx after treatment with LPS in cells with silenced *klotho* may be associated with enhanced O-GlcNAcylation, but also with the direct *klotho* knockdown-mediated decrease in plasma membrane levels of calcium TRPV2 channels [28]. On the other hand, downregulated zinc level is probably linked with *klotho* deficiency [29]. Continuing, enhanced O-GlcNAcylation led to abnormal NF-κB transcriptional activation and thus contributed to inflammation-associated complications observed in this study. However, upregulation of

inflammatory cytokines could be driven also via ROS-mediated NF-κB-dependent and -independent pathways or zinc downregulation. Response to LPS challenge in *klotho* silenced fibroblasts was manifested by increased secretion of pro-inflammatory TNFα, IL-6, IL-1β and inhibited secretion of anti-inflammatory IL-10. Klotho anti-inflammatory properties were already partially described. It was shown to suppress RIG-I-mediated inflammation and inhibit expression of IL-6 and IL-8 [30], but also to negative regulate the production of NF-κB-linked inflammatory proteins through the mechanism that involves phosphorylation of Ser536 in the transactivation domain of RelA [25]. Here, we provide evidence for klotho regulatory function in the LPS-mediated secretion of IL-10, which was identified as a modulator of inflammatory reaction due to its activity in downregulating levels of pro-inflammatory cytokines. This observation is also significantly important in terms of wound healing process, since the prolonged elevation of IL-1β and TNFα, not inhibited by IL-10 and perhaps other anti-inflammatory cytokines, may elongate the inflammatory phase and if continued, wound could enter a chronic state and fail to heal. Observed excessive inflammatory cytokines secretion, oxidative stress and activation of O-GlcNAc protein modification was correlated with the induction of unfolded protein response (UPR) in LPS-treated fibroblasts with *klotho* depletion. UPR is considered as a cellular stress response activated after the accumulation of toxic, unfolded or misfolded proteins in ER lumen seeking to restore normal functioning of ER [31]. Enhanced O-GlcNAcylation may be however not only a trigger for UPR and ER stress but also its consequence [32] and in positive feedback loop may intensify protein misfolding. Further, in this study, we observed downregulated levels of intracellular calcium, which are required by majority proteins for proper folding. Therefore, accumulation of misfolded proteins may be also due to the lack of calcium. As the response, activation of PERK/eIF2a-mediated branch of UPR was confirmed by us. PKR-like ER kinase upon ER stress dissociates from dysfunctional complex and phosphorylates eIF2a, which is a key component of 43S translation-initiation complex crucial for general mRNA translation inhibition, global protein synthesis decrease and ER load reduction [31]. This mechanism is also involved in the direct promotion of NF-κB activation and thus in ER stress-mediated inflammation [33]. However, once the ER stress intensity reaches its threshold, PERK represses adaptive response and initiates apoptosis through blockage of anti-apoptotic miRNAs [34] and control of CHOP transcription factor [34]. Therefore, PERK, although promotes cell survival, is also identified as molecular switch and apoptosis executioner during ER stress. In this study, in *klotho* deficient fibroblasts treated with LPS we observed elevated levels of active caspase 3 and downregulated Bcl-2, which confirms that accumulated protein and DNA damage was too severe and cells did not activate prosurvival adaptive responses but activated apoptotic cell death. Furthermore, we confirmed upregulated levels of molecular chaperone calnexin, which was also linked with ER stress-induced apoptosis, since it acts as a scaffold for the cleavage of Bab31 protein by caspase 8 under ER stress [35]. Apoptosis, as well as ER stress, were linked with genomic instability and micronuclei formation [36], what we also confirmed in this study. However, here we directly provide novel evidence that *klotho* plays a crucial role in genomic stability maintenance as well as prevention of ER stress and autophagy. Additionally, in this study, we observed not only apoptotic cell death in *klotho* deficient fibroblasts after treatment with LPS, but also G0/G1 cell cycle arrest, perhaps due to the genotoxicity [37] or UPR-induced accumulation of p27 [38]. It confirms, that accumulated damage leads to cell cycle arrest to allow time for repair, however it is too severe and redirects cells to the apoptotic pathway. Additionally, DNA double strand brakes sequestered in micronuclei do not activate DNA damage response pathways with the same efficiency as breaks included in the cell nucleus [39]. Since we observed most of the γH2AX staining localized in micronuclei it confirms direction to the apoptosis pathway. In terms of overall wound healing process, enhanced apoptosis not only causes impaired process but also can aggravate tissue damage that occurs during injury. Further, such non-healing wound, detained in one or more of the phases, may lead to chronic wound development. Also, the host's immune response to the presence of endotoxins prolongs inflammation and may result in severe skin and general immune disorders.

In conclusion, in this study, we show for the first time, that *klotho* silencing in fibroblasts intensified LPS-induced oxidative stress and inflammatory response, what resulted in genomic instability, ER stress and led to retardation of prosurvival autophagy and induction of apoptotic cell death. As consequence in vitro wound healing process was significantly impaired and inhibited. Therefore, these results indicate new, important role of klotho protein in modulating ER-signaling crosstalk between autophagy and apoptosis induced by LPS during the wound healing process challenged with LPS.

**Acknowledgements** The authors would like to thank Slawomir Nowak, MSc for providing antibodies against HMOX-1 and HMOX-2.

**Author contributions** JM: performed the experiments, analyzed the data, carried out data interpretation, wrote the paper, conceived and designed the experiments; PS: performed the experiments, analyzed

the data, carried out data interpretation; MK: conceived and designed the experiments; carried out data interpretation.

## Compliance with ethical standards

**Conflict of interest** The authors declare no competing interests.

## References


1. Gonzalez AC, Costa TF, Andrade ZA, Medrado AR (2016) Wound healing—a literature review. An Bras Dermatol 91:614–620
2. Ataide JA, Cefali LC, Croisfelt FM, Shimojo AAM, Oliveira-Nascimento L, Mazzola PG (2018) Natural actives for wound healing: a review. Phytother Res. https://doi.org/10.1002/ptr.6102
3. Yang H, Hu C, Li F, Liang L, Liu L (2013) Effect of lipopolysaccharide on the biological characteristics of human skin fibroblasts and hypertrophic scar tissue formation. IUBMB Life 65:526–532
4. Brothers KM, Stella NA, Hunt KM, Romanowski EG, Liu X, Klarlund JK, Shanks RM (2015) Putting on the brakes: bacterial impediment of wound healing. Sci Rep 5:14003
5. Eslani M, Movahedan A, Afsharkhamseh N, Sroussi H, Djalilian AR (2014) The role of toll-like receptor 4 in corneal epithelial wound healing. Invest Ophthalmol Vis Sci 55:6108–6115
6. He Z, Gao Y, Deng Y, Li W, Chen Y, Xing S, Zhao X, Ding J, Wang X (2012) Lipopolysaccharide induces lung fibroblast proliferation through Toll-like receptor 4 signaling and the phosphoinositide3-kinase-Akt pathway. PLoS ONE 7:e35926
7. Cheng R, Choudhury D, Liu C, Billet S, Hu T, Bhowmick NA (2015) Gingival fibroblasts resist apoptosis in response to oxidative stress in a model of periodontal diseases. Cell Death Discov 1:15046
8. Levine B, Mizushima N, Virgin HW (2011) Autophagy in immunity and inflammation. Nature 469:323–335
9. de Bentzmann S, Polette M, Zahm JM, Hinnrasky J, Kileztky C, Bajolet O, Klossek JM, Filloux A, Lazdunski A, Puchelle E (2000) Pseudomonas aeruginosa virulence factors delay airway epithelial wound repair by altering the actin cytoskeleton and inducing overactivation of epithelial matrix metalloproteinase-2. Lab Invest 80:209–219
10. Zhu Z, Dai J, Liao Y, Wang T (2017) Sox9 protects against human lung fibroblast cell apoptosis induced by LPS through activation of the AKT/GSK3beta pathway. Biochemistry 82:606–612
11. Rovetta F, Stacchiotti A, Consiglio A, Cadei M, Grigolato PG, Lavazza A, Rezzani R, Aleo MF (2012) ER signaling regulation drives the switch between autophagy and apoptosis in NRK-52E cells exposed to cisplatin. Exp Cell Res 318:238–250
12. Yamashita K, Yotsuyanagi T, Yamauchi M, Young DM (2014) Klotho mice: a novel wound model of aged skin. Plast Reconstr Surg Glob Open 2:e101
13. Chen K, Zhou X, Sun Z (2015) Haplodeficiency of *Klotho* gene causes arterial stiffening via upregulation of scleraxis expression and induction of autophagy. Hypertension 66:1006–1013
14. Banerjee S, Zhao Y, Sarkar PS, Rosenblatt KP, Tilton RG, Choudhary S (2013) Klotho ameliorates chemically induced endoplasmic reticulum (ER) stress signaling. Cell Physiol Biochem 31:659–672
15. Mytych J, Wos I, Solek P, Koziorowski M (2017) Protective role of klotho protein on epithelial cells upon co-culture with activated or senescent monocytes. Exp Cell Res 350:358–367
16. Mytych J, Romerowicz-Misielak M, Koziorowski M (2018) Klotho protects human monocytes from LPS-induced immune impairment associated with immunosenescent-like phenotype. Mol Cell Endocrinol 470:1–13
17. Yamauchi M, Hirohashi Y, Torigoe T, Matsumoto Y, Yamashita K, Kayama M, Sato N, Yotsuyanagi T (2016) Wound healing delays in alpha-Klotho-deficient mice that have skin appearance similar to that in aged humans—study of delayed wound healing mechanism. Biochem Biophys Res Commun 473:845–852
18. Liu QF, Ye JM, Deng ZY, Yu LX, Sun Q, Li SS (2015) Ameliorating effect of Klotho on endoplasmic reticulum stress and renal fibrosis induced by unilateral ureteral obstruction. Iran J Kidney Dis 9:291–297
19. Xie B, Zhou J, Shu G, Liu DC, Chen J, Yuan L (2013) Restoration of klotho gene expression induces apoptosis and autophagy in gastric cancer cells: tumor suppressive role of klotho in gastric cancer. Cancer Cell Int 13:18
20. Mytych J, Lewinska A, Bielak-Zmijewska A, Grabowska W, Zebrowski J, Wnuk M (2014) Nanodiamond-mediated impairment of nucleolar activity is accompanied by oxidative stress and DNMT2 upregulation in human cervical carcinoma cells. Chem Biol Interact 220:51–63
21. Martin M, Leffler J, Smolag KI, Mytych J, Bjork A, Chaves LD, Alexander JJ, Quigg RJ, Blom AM (2016) Factor H uptake regulates intracellular C3 activation during apoptosis and decreases the inflammatory potential of nucleosomes. Cell Death Differ 23:903–911
22. Thome MP, Filippi-Chiela EC, Villodre ES, Migliavaca CB, Onzi GR, Felipe KB, Lenz G (2016) Ratiometric analysis of Acridine Orange staining in the study of acidic organelles and autophagy. J Cell Sci 129:4622–4632
23. Kostarnoy AV, Gancheva PG, Logunov DY, Verkhovskaya LV, Bobrov MA, Scheblyakov DV, Tukhvatulin AI, Filippova NE, Naroditsky BS, Gintsburg AL (2013) Topical bacterial lipopolysaccharide application affects inflammatory response and promotes wound healing. J Interferon Cytokine Res 33:514–522
24. Ravikumar P, Ye J, Zhang J, Pinch SN, Hu MC, Kuro-o M, Hsia CC, Moe OW (2014) Alpha-Klotho protects against oxidative damage in pulmonary epithelia. Am J Physiol Lung Cell Mol Physiol 307:L566–L575
25. Zhao Y, Banerjee S, Dey N, LeJeune WS, Sarkar PS, Brobey R, Rosenblatt KP, Tilton RG, Choudhary S (2011) Klotho depletion contributes to increased inflammation in kidney of the db/db mouse model of diabetes via RelA (serine)536 phosphorylation. Diabetes 60:1907–1916
26. Six I, Okazaki H, Gross P, Cagnard J, Boudot C, Maizel J, Drueke TB, Massy ZA (2014) Direct, acute effects of Klotho and FGF23 on vascular smooth muscle and endothelium. PLoS One 9:e93423
27. Kitano T, Yamada H, Kida M, Okada Y, Saika S, Yoshida M (2017) Impaired healing of a cutaneous wound in an inducible nitric oxide synthase-knockout mouse. Dermatol Res Pract 2017:2184040
28. Lin Y, Sun Z (2012) Antiaging gene Klotho enhances glucose-induced insulin secretion by up-regulating plasma membrane levels of TRPV2 in MIN6 beta-cells. Endocrinology 153:3029–3039
29. Miyazaki T, Takenaka T, Inoue T, Sato M, Eiki Y, Nodera M, Hanyu M, Ohno Y, Shibazaki S, Suzuki H (2009) Zinc deficiency may accelerate aging by inhibiting klotho mRNA expression. Trace Nut Res 26:74–78
30. Liu F, Wu S, Ren H, Gu J (2011) Klotho suppresses RIG-I-mediated senescence-associated inflammation. Nat Cell Biol 13:254–262
31. Bravo R, Parra V, Gatica D, Rodriguez AE, Torrealba N, Paredes F, Wang ZV, Zorzano A, Hill JA, Jaimovich E, Quest AF, Lavandero S (2013) Endoplasmic reticulum and the unfolded protein response: dynamics and metabolic integration. Int Rev Cell Mol Biol 301:215–290
32. Wang ZV, Deng Y, Gao N, Pedrozo Z, Li DL, Morales CR, Criollo A, Luo X, Tan W, Jiang N, Lehrman MA, Rothermel BA, Lee AH, Lavandero S, Mammen PP, Ferdous A, Gillette TG, Scherer

PE, Hill JA (2014) Spliced X-box binding protein 1 couples the unfolded protein response to hexosamine biosynthetic pathway. Cell 156:1179–1192
33. Schmitz ML, Shaban MS, Albert BV, Gokcen A, Kracht M (2018) The crosstalk of endoplasmic reticulum (ER) stress pathways with NF-kappaB: complex mechanisms relevant for cancer, inflammation and infection. Biomedicines 6:58
34. Chen Y, Brandizzi F (2013) IRE1: ER stress sensor and cell fate executor. Trends Cell Biol 23:547–555
35. Delom F, Emadali A, Cocolakis E, Lebrun JJ, Nantel A, Chevet E (2007) Calnexin-dependent regulation of tunicamycin-induced apoptosis in breast carcinoma MCF-7 cells. Cell Death Differ 14:586–596
36. Kalsbeek D, Golsteyn RM (2017) G2/M-phase checkpoint adaptation and micronuclei formation as mechanisms that contribute to genomic instability in human cells. Int J Mol Sci 18:2344
37. Tudzarova S, Mulholland P, Dey A, Stoeber K, Okorokov AL (2016) G.H. Williams, p53 controls CDC7 levels to reinforce G1 cell cycle arrest upon genotoxic stress. Cell Cycle 15:2958–2972
38. Han C, Jin L, Mei Y, Wu M (2013) Endoplasmic reticulum stress inhibits cell cycle progression via induction of p27 in melanoma cells. Cell Signal 25:144–149
39. Terradas M, Martin M, Tusell L, Genesca A (2009) DNA lesions sequestered in micronuclei induce a local defective-damage response. DNA Repair 8:1225–1234